Astron. Astrophys. 329, 1019–1027 (1998)

ASTRONOMY AND ASTROPHYSICS

Spectral analysis of the extreme helium star LSS 3184⋆

J.S. Drilling[1], **C.S. Jeffery**[2], **and U. Heber**[3]

[1] Department of Physics and Astronomy, Louisiana State University, Baton Rouge, Louisiana 70803, USA
[2] Armagh Observatory, College Hill, Armagh BT61 9DG, Northern Ireland
[3] Dr. Remeis-Sternwarte, Universität Erlangen-Nürnberg, D-96049 Bamberg, Germany

Received 17 October 1996 / Accepted 14 August 1997

Abstract. LSS 3184 is a hydrogen-deficient, early B-type giant, recently found to pulsate with a period of 2.5 hours. Its photospheric parameters have been derived from optical high-resolution spectra by the method of fine analysis. The principal results are $T_{\rm eff}$ = 23 300 K, $\log g$ = 3.35, $n_{\rm H}/\,n_{\rm He} \lesssim 0.00015$, $n_{\rm C}/\,n_{\rm He}$ = 0.003, $n_{\rm N}/\,n_{\rm He}$ = 0.0005, and $n_{\rm O}/\,n_{\rm He}$ = 0.0003. Hydrogen is extremely deficient. The effective temperature is consistent with broad-band visual and ultraviolet spectrophotometry and an extinction $E_{\rm B-V} \sim 0.27$. Its previous evolution is reflected in the chemistry of the atmosphere, which contains enriched nitrogen from CNO-cycle hydrogen burning, and carbon from 3α helium burning. Thus LSS 3184 is a true extreme helium star with a composition similar to BD$-9°4395$.

With $T_{\rm eff}$, $\log g$, and pulsation properties very similar to the C-poor and N-rich helium star V652 Her, evolutionary mechanisms which can result in very different surface compositions for the two stars must be examined.

Key words: stars: helium – individual (LSS 3184) – abundances – chemically peculiar – emission line: Be

1. Introduction

The star LSS 3184 was found to be hydrogen-deficient by Drilling (unpublished) during a spectroscopic survey of OB^+ stars in the Southern Milky Way (Drilling 1980). It was subsequently observed photometrically and the broad-band colours were used to estimate the reddening, $E_{\rm B-V}$ = 0.26, and to derive an effective temperature $T_{\rm eff}$ = 21 700 K (Heber et al. 1986). A preliminary fine analysis by Heber et al. (1986) yielded $T_{\rm eff}$ = 22 000 K and $\log g$ = 3.2, and showed nitrogen to be overabundant by a factor of about 50. The purpose of the present paper is to give the final results and details of the fine analysis, and to present unpublished results on low-resolution ultraviolet spectroscopy.

2. Observations

A blue-visual spectrum of LSS 3184 was obtained using CASPEC, a Cassegrain échelle spectrograph, on the ESO 3.6m telescope at La Silla, Chile, at approximately UT 02:00, 1985 April 8. The 3600 second exposure covered the wavelength range from 3800 to 4800 Å at a resolution of 0.5 Å and a S/N of 30. The data reduction has been described by Heber et al. (1986). Low-resolution spectra (image numbers LWP 8966, LWP 8967, and SWP 29087) obtained with IUE on 1986, August 30 and extracted from the Uniform Low Dispersion Archive at the Rutherford Appleton Laboratory have also been used in this investigation. The SWP data have been corrected for sensitivity degradation of the camera and geocoronal Lyα emission has been removed. The LWP data have been filtered to remove noisy data. An inspection of the CASPEC spectrum shows immediate similarities with the well-studied spectrum of the EHe star V652 Her = BD+13°3224 (Jeffery & Hill 1986; Jeffery et al. 1986), and the line identifications for this star proved very helpful in completing the line identifications for LSS 3184.

Equivalent widths (W_λ) were measured for all lines identified. Measurements were made relative to a local continuum defined by small regions of spectrum between absorption lines within ±20Å of the line being measured, this being of similar dimension to a single CASPEC échelle order. Equivalent widths were measured both by direct integration and by integrating a Gaussian fitted to the line profile after cleaning local defects such as cosmic rays or weak blends in one or other wing. Both measures normally agreed to within ±10%. For close blends due to the same ion, the equivalent width of the blend was measured. Where blends could be resolved into two or more components, a multiple Gaussian was fitted and the equivalent width of each Gaussian was recorded. This procedure was successful in reproducing the equivalent width of the entire blend and the relative strengths of the individual components. After the analysis had been completed, we found to our great embarassment that we had obtained a second, similar spectrum at UT 03:38

Send offprint requests to: J.S. Drilling

⋆ Based on observations obtained at the European Southern Observatory, La Silla, Chile, and with the IUE satellite retrieved from the IUE archive at the World Data Centre, Rutherford Appleton Laboratory, UK

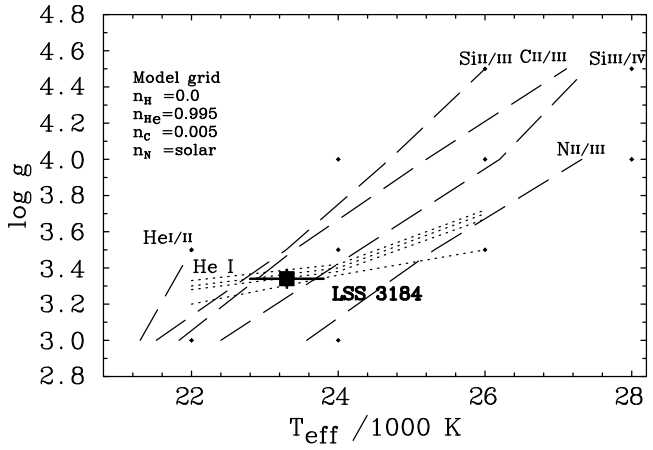

Fig. 1. The adopted model atmosphere for LSS 3184 is shown relative to the loci of ionisation equilibria and He I line-profile fits in the $\{T_{\rm eff}, \log g\}$ plane. The ionisation equilibria for He I/II, C II/III, N II/III, Si II/III and Si III/IV are shown as broken lines. The best fits to the HeI line profiles are shown as dotted lines. Solid diamonds indicate the grid of line-blanketed model atmospheres.

on April 8. This spectrum provided us with an external check, and measurements of selected lines agreed to within $\pm 10\%$. The principal source of error remains continuum placement. A few lines were measured independently by two authors, again agreeing to within $\pm 10\%$.

3. Photospheric parameters

The procedure adopted here has been to determine $T_{\rm eff}$ from the ionisation equilibria of prominent ions, along with other atmospheric properties, and to verify subsequently that these are consistent with the continuous flux distribution.

The LTE line-blanketed model atmospheres and the line-formation codes used in this analysis are described by Möller (1990) and by Jeffery & Heber (1992). The important feature of these models is that line-blanketing is treated using opacity distribution functions calculated from the Kurucz & Peytremann (1975) list of 265 000 lines, in the same manner as adopted in Kurucz's stellar atmosphere program ATLAS6 (cf. Kurucz 1979). Previously, Heber et al. (1986) had considered the blanketing effect of 800 He I and metal lines. The continuous opacities are nearly the same as those adopted by Kurucz (1979), with the addition of carbon and nitrogen from Peach (1970). A plane-parallel approximation is justified since the density scale height in the atmosphere is still small ($< 2\%$) compared to the stellar radius, even for the lowest gravity models considered.

Since the hydrogen abundance ($n_{\rm H}$) in LSS 3184 is small and $T_{\rm eff}$ is to be obtained from the ionisation equilibrium alone, the procedure for obtaining a model atmosphere for LSS 3184 involves only five free parameters, being $T_{\rm eff}$, the surface gravity ($\log g$), the microturbulent velocity ($v_{\rm t}$), the carbon abundance ($n_{\rm C}$), and the nitrogen abundance ($n_{\rm N}$).

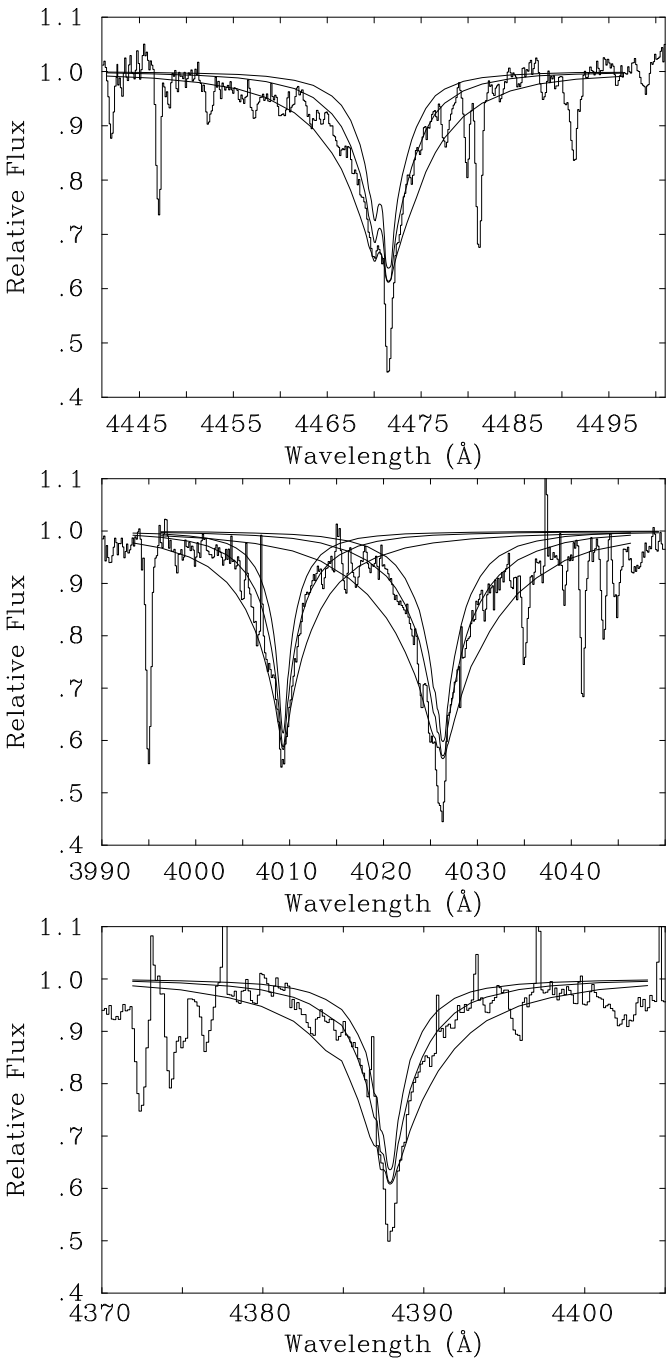

Fig. 2. Theoretical models for observed He I line profiles in LSS 3184 calculated for model atmospheres with $n_{\rm H} = 0.0001$ and with $T_{\rm eff} = 24\,000$K, $\log g = 3.0$, $n_{\rm C} = 0.005$ (top), $T_{\rm eff} = 23\,300$K, $\log g = 3.35$, $n_{\rm C} = 0.003$ (middle), and $T_{\rm eff} = 22\,000$K, $\log g = 4.0$, $n_{\rm C} = 0.005$ (bottom). Histogram: CASPEC spectrum (1985 April 6). The theoretical profiles have been convolved with an instrumental broadening profile (FWHM = 0.2 Å).

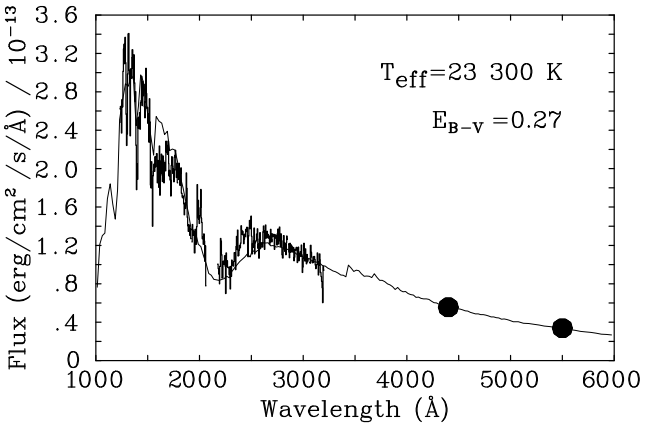

Fig. 3. Theoretical flux distribution for $T_{\rm eff}$ = 23 300K, log g = 3.35 and $E_{\rm B-V}$ = 0.27 compared with spectrophotometric observations of LSS 3184. Histogram: IUE spectrum. Filled circles: BV photometry.

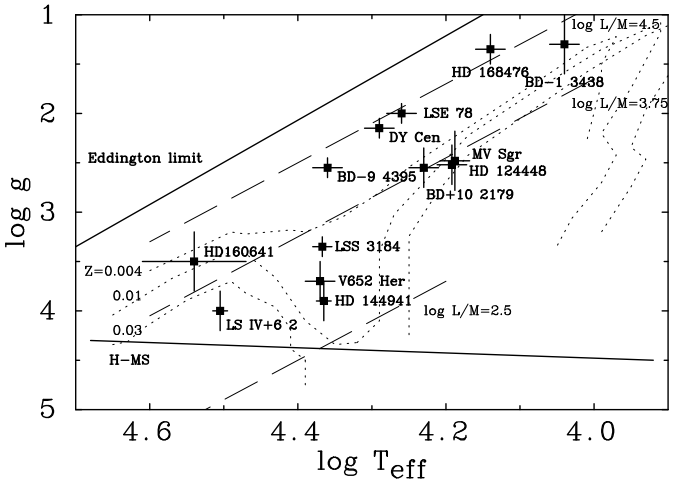

Fig. 4. The log g − log $T_{\rm eff}$ diagram for EHe (▪), stars, showing the positions of LSS 3184, the hydrogen main sequence (H-MS), and the classical (e^--scattering) Eddington limit for radiative stability. L/M loci (dashed) and pulsation instability boundaries (Saio 1995: dotted) are also shown.

3.1. Microturbulence

The microturbulence ($v_{\rm t}$) determined by constraining the abundances derived from numerous lines of C II, N II, and O II to be independent of equivalent width was $v_{\rm t}$ = 15 km s^{-1}. The uncertainty in this figure is $\sim \pm$5 km s^{-1}. The adiabatic sound-speed in the model atmosphere at the depth where the majority of these lines is formed is 12–13 km s^{-1}. $v_{\rm t}$ would appear to be slightly supersonic, but it is noted that similar and higher values were required in analyses of other helium stars (Jeffery & Heber 1992, 1993, Jeffery 1993). This is a reminder that the notion of microturbulence is useful in accounting for well-known discrepancies between theoretical and observed stellar atmospheres, but has a limited physical significance. The measured $v_{\rm t}$ also accounts for the N abundance being lower than that found by Heber et al. (1986) who adopted $v_{\rm t}$ = 5 km s^{-1}. After applying the measured instrumental broadening of 0.2 Å (FWHM) to several strong O II line profiles, it was apparent that no further line-broadening could be measured, such as might be due to rotation or pulsation. Given that each spectrum was exposed for $\sim$ 0.4 cycles, a maximum line broadening of $\sim$ 15 km s^{-1} would be superimposed by the radial pulsation (Jeffery & Hill 1996a). Since the question remains why such a large value for $v_{\rm t}$ is required in both BD−9°4395 and LSS 3184, the fact that both are high luminosity pulsators suggests there may be some correlation between pulsation and microturbulence.

3.2. Ionisation equilibrium

The ionisation equilibria of C II/C III, N II/N III, and Si II/ Si III/ Si IV were used to determine $T_{\rm eff}$ as a function of log g. In contrast to previous analyses (cf. Jeffery & Heber 1992), the Si III multiplet 2.00 lines gave results consistent with Si III multiplet 9.00, suggesting that at the higher $T_{\rm eff}$ and log g of LSS 3184, these lines can be treated successfully in LTE.

The He II λ4685.7 Å line could be measured with an equivalent width of 67 mÅ. This was well below the strength expected for the $T_{\rm eff}$ indicated by other ions. The line shape appears to be approximately triangular, and noticably different from other isolated absorption lines and is similar in both CASPEC spectra. However there is no satisfactory explanation for this discrepancy in line strength.

3.3. Surface gravity

Line profiles were calculated for He I λ4009 Å, He I λ4026 Å, He I λ4121 Å, He I λ4387 Å, and He I λ4471 Å in order to determine log g as a function of $T_{\rm eff}$. The non-diffuse line He I λ4121 Å is blended with nearby lines and relatively insensitive to surface gravity, so was not considered further. The coincidence of the He I line fits and the ionisation equilibria for C II/III and Si II/III/IV was used to determine the overall model parameters (Fig. 1). The N II/III equilibrium shown in Fig. 1 is based on four weak N III lines, with implied abundances spread over 1 dex, and is considered unreliable. The N II lines, however, provide an excellent measure of the N abundance, $n_{\rm N}/\,n_{\rm He}$ = 0.0005. At $T_{\rm eff}$ = 23 300 K and log g = 3.35, the fits for He I λ4471 Å, He I λ4387 Å, He I λ4009 Å and He I λ4026 Å (Fig. 2) are in excellent agreement with the observations. However it is noted that at the gravity and temperature of LSS 3184, the density in the atmosphere where the helium lines are formed is at the upper limit of the available line-broadening tables (Barnard et al., 1969, 1974, 1975). Publication of the excellent extension of He I broadening calculations to higher and lower densities and to additional lines by Beauchamp et al. (1996) is eagerly anticipated.

3.4. Atmospheric parameters

The atmospheric parameters obtained for LSS 3184 are thus $T_{\rm eff}$ = 23 300 ± 700 K, log g = 3.35 ± 0.1, $n_{\rm C}$ = 0.003 ±

0.001, $n_{\rm N}$ = 0.0005 $\pm$ 0.0002, and $v_{\rm t}$ = 15 $\pm$ 5km/s. These, with $n_{\rm H}$=0.0001 and solar abundances for other atomic species, were adopted to calculate the final model atmosphere used to derive the remaining properties. The location of LSS 3184 in the $\{T_{\rm eff}, \log g\}$ plane is shown in Fig. 4. For a star with this gravity, $\log(L/M)$ = 3.52 $\pm$ 0.15 (solar units). Assuming that the stellar interior consists of a degenerate CO core surrounded by a luminous He-burning shell, a core mass $M \approx 0.55\,{\rm M}_{\odot}$ may be estimated (Jeffery 1988), but this is at the extreme lower-limit of validity of the core-mass shell-luminosity relation.

3.5. Spectrophotometry

Having obtained the atmospheric parameters for LSS 3184 by the method of fine analysis, it remains to check that $T_{\rm eff}$ is consistent with the spectrophotometry. All IUE low-resolution images were extracted from the Uniform Low Dispersion Archive and an average spectrum weighted by the respective exposure times was formed. There is no significant variation in flux between images obtained with the same camera at different times. The flux-calibrated spectrum and the published Johnson B and V magnitudes (Drilling & Hill, 1986) were compared with the model flux distributions reddened by varying amounts. For $T_{\rm eff}$ = 23 300K and $\log g$ = 3.35, a reddening of $E_{\rm B-V}$ = 0.27 $\pm$ 0.02 gave the best agreement between model and observation, as shown in Fig. 3. A variation of $\pm$0.05 in $E_{\rm B-V}$ corresponds roughly to a variation of $\pm$2000 K in $T_{\rm eff}$. Small discrepancies between theoretical and observed fluxes may be due to insufficient line opacity (1600Å), noise (2000Å) and a non-standard width in the 2175Å interstellar band (2400Å).

3.6. Photospheric abundances

The line abundances for other ions were obtained by comparing equivalent widths with individual curves of growth. In general, only lines found to be largely free from blends are shown in Table 1. In addition, for carbon lines, a critical selection excluded all lines which were either very strong (non-LTE), very weak (measurement errors), contaminated by any blend or cosmic ray, or for which there were uncertainties in the atomic data. The individual line abundances are shown in Table 1. The mean abundance for each ion is given with the standard deviation about the mean.

All three Balmer lines in our spectra are blended with lines of S, Si, and C, respectively. An upper limit for the hydrogen abundance of $n_{\rm H} \lesssim 0.0006 \pm 0.0003$ is obtained assuming no contribution from the blending lines. For Hγ, this limit can be reduced to $n_{\rm H} \lesssim 0.00015$ by considering the S III$_4$ component of the blend.

The final photospheric abundances are shown in Table 2, alongside results obtained for V652 Her (Jeffery et al. 1986), for BD$-9^{\circ}4395$ (Jeffery & Heber 1992), for HD144941 (Harrison & Jeffery 1996), and for the Sun (Anders & Grevesse 1989). Where data are available for more than one ion of a species in Table 1, these have been combined to form the mean values given in Table 2.

3.7. Time-dependent behaviour

The preliminary surface parameters derived by Heber et al. (1986) for LSS 3184 were similar to those of the pulsating helium star V652 Her, prompting Saio (1995) to predict that LSS 3184 should also pulsate with a period of 0.1 days, as subsequently verified by Kilkenny & Koen (1995). Since the pulsation period of LSS 3184 ($\sim$ 155min) is fairly short compared with the exposure times of our spectra (60min), the effects of pulsation on the measured line profiles and the assumption of hydrostatic equilibrium in the model atmospheres need to be considered.

A preliminary measurement of the velocity curve (Jeffery & Hill 1996a) indicates that line broadening over 60 min. can not be much more than 15 km/s, which is equivalent to the instrumental broadening. Further observations to estimate the amplitude of the temperature variation are in progress. Studies of the larger amplitude variable V652 Her (Jeffery & Hill 1986) indicate that the hydrostatic approximation provides a sufficient description of the stellar atmosphere through 90% of the pulsation cycle. At minimum radius, rapid outward acceleration of the atmosphere increases the effective surface gravity by $\sim$ 1dex. Such rapid acceleration is not seen in LSS 3184 (Jeffery & Hill 1996a), and thus the atmosphere is assumed to be in hydrostatic equilibrium throughout the pulsation cycle.

3.8. Errors

Uncertainties in the final abundances arise from a number of possible sources including the placement of the continuum in measuring line profiles and equivalent widths, errors in $T_{\rm eff}$, $\log g$, $v_{\rm t}$ and $n_{\rm C}$ for the final model, errors in atomic data used for the analysis of individual lines, a failure to include all continuous and line opacity sources from the model atmospheres, the neglect of convection and the assumptions of local thermodynamic and hydrostatic equilibrium and of plane-parallel geometry.

The derivatives of the mean ion abundances with respect to $T_{\rm eff}$, $\log g$, $v_{\rm t}$, $n_{\rm C}$ and W_{λ} have been established numerically and are shown in Table 3. Assuming that all five variables are independent, which they are not, the maximum error in each ion abundance can thence be estimated. For the majority of ions, these errors are smaller than the standard deviation due to several lines belonging to the same ion. It is noted that the largest errors are due to temperature sensitive lines which themselves define the measurement of $T_{\rm eff}$. Of other sources, errors in atomic data contribute in the same way as errors in W_{λ}, and are random errors associated with each multiplet. W_{λ} measurement errors are random errors associated with each line, except that continuum or background definition may produce a systematic error whose contribution is represented by $\frac{\partial \log n}{\partial \log W_{\lambda}}$ in Table 3. Assumptions made in constructing the model atmosphere may also lead to systematic errors, since these affect where and how the lines

Table 1. Photospheric line abundances for LSS 3184. References for gf-values are given with the ion designation

Ion Mult.	Ref. λ (Å)	W_λ (mÅ)	$\log gf$	$-\log n$	Notes
H I					
γ	4340.4	60		3.41	bl S III$_4$
δ	4101.7	34		3.40	bl Si III$_{8,10}$
ϵ	3970.1	63		2.90	bl C II$_{38}$
				3.24	$\pm$ 0.29
C II	Yan 87				
12.01	4637.4	55	-1.237	2.37	
12.02	4306.3	27	-1.678	2.33	
17.08	4802.7	134	-0.411	2.46	
28	4313.1	95	-0.378	2.44	
	4323.1	26	-1.108	2.46	
39	4413.3	39	-0.629	2.40	
42	4285.7	52	0.373	2.43	
				2.41	$\pm$ 0.05
C III	All 90				
1	4647.2	165	0.072	2.85	
5	4659.1	11	-0.652	2.50	
	4665.9	28	0.049	2.57	
16	4067.9	50	0.827	2.77	
				2.67	$\pm$ 0.16
N II	Bec 89				
5	4601.5	204	-0.385	3.31	
	4607.2	178	-0.483	3.37	
	4613.9	169	-0.607	3.30	
	4621.3	222	-0.483	3.10	
	4630.5	320	0.093	3.00	bl C II$_{49}$
	4643.1	198	-0.385	3.34	
12	3995.0	296	0.225	3.38	
15	4447.0	147	0.238	3.81	
20	4774.2	42	-1.056	3.27	
	4779.7	76	-0.577	3.41	
	4781.2	41	-1.036	3.30	
	4788.1	113	-0.388	3.32	
	4793.7	67	-1.056	3.01	
	4803.3	178	-0.135	3.15	
	4810.3	60	-1.036	3.09	
30	3829.8	110	-0.599	3.10	
	3842.2	97	-0.695	3.10	
	3847.4	95	-0.821	2.98	
33	4227.7	177	-0.089	3.02	
39	4035.1	127	0.597	3.68	
	4041.3	165	0.830	3.66	
	4043.5	100	0.714	3.98	
	4056.9	67	-0.461	3.07	
48	4237.0	191	0.567	3.47	bl
	4241.2	69	-0.336	3.14	
	4241.8	166	0.728	3.51	bl N II$_{47}$
	4242.4	55	-0.336	3.28	
50	4160.5	24	-1.125	2.93	
	4179.7	106	-0.204	2.98	
55	4427.2	116	-0.004	3.04	
	4428.0	89	-0.165	3.08	bl Mg II$_9$

Table 1. (continued)

Ion Mult.	Ref. λ (Å)	W_λ (mÅ)	$\log gf$	$-\log n$	Notes
N II	contd.				
	4431.8	73	-0.165	3.21	
	4432.7	139	0.583	3.47	
	4433.5	92	-0.040	3.18	bl Mg II$_9$
	4442.0	82	0.312	3.61	
58	4530.4	157	0.671	3.41	bl N III$_3$
61	4678.1	124	0.079	3.00	
				3.27	$\pm$ 0.25
N III	But 84				
2	4640.6	32	0.140	3.58	
3	4514.9	22	0.225	2.85	
	4523.6	11	-0.353	2.72	
	4534.6	15	-0.458	2.42	
				2.89	$\pm$ 0.49
O II	Bel 94				
1	4638.9	152	-0.307	3.28	bl C II$_{12.01}$
	4650.8	86	-0.331	3.75	
	4661.6	111	-0.249	3.63	
	4676.2	74	-0.360	3.82	
2	4319.6	85	-0.357	3.78	
	4345.6	102	-0.330	3.66	bl N III$_{10}$
	4349.4	152	0.086	3.71	
	4366.9	61	-0.320	4.03	
5	4414.9	136	0.210	3.83	
	4452.4	52	-0.757	3.57	
6	3945.0	87	-0.699	3.36	
	3954.4	159	-0.396	3.12	bl Fe III$_{120}$
	3973.3	176	0.009	3.39	$*$ bl C II$_{37,38}$
	3982.7	78	-0.682	3.44	
10	4069.9	137	0.365	3.83	bl C III$_{16}$
	4072.2	125	0.545	3.75	
	4078.8	45	-0.272	3.68	
	4085.1	64	-0.175	3.56	
	4092.9	15	-0.306	4.21	$*$ wk
	4094.1	21	-1.469	2.88	
11	3907.5	35	-0.924	3.19	
12	3847.9	78	-1.066	2.57	bl Mg II$_5$
	3850.8	43	-1.076	2.93	bl Mg II$_5$
	3851.0	88	-0.854	2.69	
	3863.5	14	-0.971	3.61	
	3882.2	74	-0.032	3.63	
15	4591.0	83	0.346	3.81	
	4596.2	96	0.196	3.55	
16	4351.3	93	0.228	3.65	bl N III$_{10}$
17	3912.0	99	0.000	3.50	
19	4132.8	82	-0.122	3.39	
20	4097.3	135	-0.604	3.17	$*$ bl O II$_{48}$
	4104.7	86	-0.143	3.77	
	4119.2	89	0.453	3.90	
21	4112.0	69	-0.561	3.07	
25	4705.4	76	0.519	3.89	
	4741.7	23	-0.928	3.14	
26	4395.9	61	-0.183	3.40	bl Fe III$_4$

Table 1. (continued)

Ion Mult.	Ref. λ (Å)	W_λ (mÅ)	log gf	$-\log n$	Notes
O II	contd.				
34	3821.5	25	-1.027	3.08	
36	4185.5	63	0.610	3.70	
	4189.8	95	0.723	3.51	bl S II$_{44}$
40	4703.2	33	0.274	3.64	
42	4192.5	27	-0.325	3.24	
48	4108.8	11	-0.161	3.82	
50	4062.9	19	-0.148	3.57	
67	4276.7	70	-0.717	2.20	∗ bl O II$_{54}$
	4275.6	71	0.766	3.66	
86	4489.5	15	0.587	4.30	∗ wk
	4491.2	196	0.842	2.75	
93	4609.4	35	0.709	3.93	
97	4060.6	48	0.775	3.77	
101	4253.9	165	0.929	2.47	∗ bl S III$_4$
				3.50	± 0.35
Ne II	Wie 66				
56	4379.5	18	0.468	2.61	∗ bl N III$_{18}$
56	4430.9	40	0.246	1.76	∗ bl Fe III$_4$
Mg II	Wie 69				
4	4481.1		0.568		⎤
	4481.2	236	0.732	4.30	⎦
10	4384.7	9	0.166	4.31	
	4390.6	11	0.316	4.50	
				4.37	± 0.11
Al III	Kod 70				
3	4512.5	88	0.405	5.57	
	4528.9		-0.282		⎤
	4529.1	143	0.670	5.47	⎦
5	4149.9	99	0.619	5.39	
8	4479.9		0.894		⎤
	4480.0	107	1.021	5.58	⎦
				5.50	±0.09
Si II	Bec 90				
1	3853.7	8	-1.377	4.38	
1	3862.6	19	-0.682	4.69	
3	4128.1	190	0.369	3.61	∗ bl
3	4130.9	58	0.545	4.62	
				4.56	±0.16
Si III	Har 70				
2	4567.8	204	0.061	4.85	
2	4574.8	165	-0.416	4.61	
3	4338.5	30	-1.143	5.03	
8.09	4716.7	80	0.491	4.55	∗ bl S II$_9$
9	4813.3	56	0.702	4.83	
9	4819.7	80	0.814	4.71	
13	4683.0	18	0.185	4.55	
				4.76	±0.18
Si IV	Bec 90				
1	4116.1	81	-0.103	4.51	
5	4212.4	17	0.804	4.15	
				4.33	±0.25

Table 1. (continued)

Ion Mult.	Ref. λ (Å)	W_λ (mÅ)	log gf	$-\log n$	Notes
P III	Wie 69				
3	4222.2	45	0.190	6.66	
	4246.7	34	-0.119	6.50	
				6.58	±0.11
S II	Wie 69				
9	4815.5	51	-0.050	4.15	?
44	4217.2	41	-0.150	3.62	∗
				4.15	
S III	Har 70, Wie 69				
4	4285.0	77	-0.046	5.14	
	4361.5	44	-0.724	4.81	∗ bl C III$_{50}$
7	4354.6	53	-1.602	3.84	∗
8	3928.6	44	-0.160	5.45	∗ bl He I$_{58}$
	3983.8	75	-0.438	4.82	
	3986.0	58	-0.790	4.65	
				4.87	±0.25
Fe III	Kur 75				
4	4419.6	36	-2.301	5.50	
118	4137.9	18	0.644	5.18	
	4139.4	16	0.553	5.14	
	4140.5	13	0.114	4.80	
	4164.8	78	0.940	4.67	
	4166.9	25	0.436	4.81	
				5.02	±0.31

Notes:

⎤	. . .
⎦	Line abundance calculated from blend
bl	Blend with weak line from another species
∗	Line omitted from mean abundance
∗ bl	Blended line omitted . . .

References:

All 90	Allard et al. 1990
Bec 89	Becker & Butler 1989
Bec 90	Becker & Butler 1990
Bel 94	Bell et al. 1994
But 84	Butler 1984
Har 70	Hardorp & Scholz 1970
Kod 70	Kodaira & Scholz 1970
Kur 75	Kurucz & Peytremann 1975
Wie 66	Wiese et al. 1966
Wie 69	Wiese et al. 1969
Yan 87	Yan et al. 1987

are formed. Quantifying these will require the construction of new model atmospheres which have not yet been successfully attempted.

4. LSS 3184 and other EHe stars

The comparison provided by Table 2 demonstrates that LSS 3184 has a composition which is similar to that of the extreme helium star BD−9°4395. The H, He and CNO abun-

Table 2. Model parameters and photospheric abundances for LSS 3184. Abundances are normalised to $\log \sum_i \mu_i n_i$ = 12.15. Comparisons are given for V652 Her, BD-9°4395, HD 144941 and the Sun.

	LSS 3184	V652 Her	BD-9° 4395	HD 144941	Sun
$T_{\rm eff}$	$23\,300 \pm 700$	23 500	22 700	23 200	
$\log g$	3.35 ± 0.10	3.7	2.55	3.9	
$v_{\rm t}$	15 ± 5		20		
H	≤ 7.72	9.5	8.74	10.28	12.00
He	11.54	11.54	11.54	11.54	10.99
C	9.02 ± 0.23	7.03	9.17	6.80	8.58
N	8.26 ± 0.25	8.9	7.97	6.5	8.05
O	8.05 ± 0.36	7.9	7.90	7.0	8.93
Mg	7.17 ± 0.11	8.1	7.25	6.1	7.58
Al	6.04 ± 0.09	6.7	5.55	4.8	6.47
Si	6.91 ± 0.24	7.7	7.83	6.0	7.55
P	4.96 ± 0.11	5.8	6.21		5.45
S	6.67 ± 0.25	7.4	7.83		7.21
Fe	6.52 ± 0.31	7.4	6.57	6.4	7.48

References:

V652 Her	Jeffery et al. 1986;
	$T_{\rm eff}$, $\log g$: Lynas-Gray et el. 1984;
	O,Ne,Mg,Al,P,S,Fe: Jeffery 1996
BD-9°4395	Jeffery & Heber 1992
HD 144941	Harrison & Jeffery 1997
Sun	Anders & Grevesse 1989;
	Fe: Holweger et al.1990;
	C: Stürenburg & Holweger, 1990

Table 3. Systematic errors in the mean ion abundances. The measured errors (δ) in each of $T_{\rm eff}$, $\log g$, $v_{\rm t}$, $n_{\rm C}$ and W_λ are shown first. The partial abundance derivative with respect to each of these variables is shown beneath, for each ion. Assuming that the errors are independent and random, then the total error ($\delta(\log n)$) shown on the right may be compared with the standard deviation ($\sigma(\log n)$) in the derived mean abundances.

	$\delta \log T_{\rm eff}$	$\delta \log g$	$\delta \log v_{\rm t}$	$\delta \log n_{\rm C}$	$\delta \log W_\lambda$		
	0.01	0.1	0.12	0.2	0.05		
Ion	$\frac{\partial \log n}{\partial \log T_{\rm eff}}$	$\frac{\partial \log n}{\partial \log g}$	$\frac{\partial \log n}{\partial \log v_{\rm t}}$	$\frac{\partial \log n}{\partial \log n_{\rm C}}$	$\frac{\partial \log n}{\partial \log W_\lambda}$	$\delta(\log n)$	$\sigma(\log n)$
H	2.82	-0.15	0.00	0.00	3.08	0.16	0.29
C II	1.73	-0.09	-0.33	-0.03	2.67	0.14	0.05
C III	-15.84	0.90	-0.61	-0.19	-8.97	0.49	0.16
N II	0.16	0.06	-1.12	0.02	2.12	0.17	0.25
N III	-16.71	0.96	-0.54	-0.21	-8.79	0.49	0.49
O II	-5.20	0.34	-0.65	-0.05	-2.16	0.15	0.35
Mg II	4.76	-0.17	-0.66	0.03	4.84	0.26	0.11
Al III	1.92	0.00	-0.80	0.01	3.08	0.18	0.09
Si II	13.10	-0.57	-0.65	0.15	11.24	0.59	0.16
Si III	-3.01	0.24	-0.84	-0.02	-0.49	0.11	0.18
Si IV	-16.41	1.04	-0.82	-0.18	-9.66	0.53	0.25
P III	-0.66	0.23	-0.26	0.00	0.76	0.05	0.11
S III	-4.63	0.42	-0.47	-0.04	-2.03	0.13	0.25
Fe III	-1.59	0.22	-0.25	-0.01	0.08	0.04	0.31

dance signature is indicative of material which has been almost entirely CNO-processed (destroying H) and partially 3α processed (producing C). The magnesium, aluminium, silicon, phosphorous and sulphur abundances are subsolar by $\sim$0.4 dex, whilst iron is subsolar by $\sim$1 dex. The extraordinary surface abundances of extreme helium stars have been discussed most recently by Jeffery (1996), where a comparison of all analyzed helium stars may be found. The fact that in LSS 3184 nitrogen is not enriched (by CNO processing) is superficially difficult to understand. Although nitrogen is destroyed by 3α burning, the admixture of carbon in LSS 3184 is relatively small, as indicated by the carbon abundance. Adopting a subsolar primordial metallicity (-0.5 dex, say) provides a natural solution since carbon is then enriched by 0.9 dex, nitrogen by 0.7 dex and oxygen is depleted by 0.4 dex.

In one sense LSS 3184 is slightly unusual because several EHes show a significant and inexplicable overabundance of phosphorous (Jeffery 1996) which is absent here. However, it should be remembered that amongst the EHes there are large star-to-star variations in the abundances of individual species. Therefore, in view of its abundances, LSS 3184 may be properly considered to be a true extreme helium star and carries significance as having the highest gravity and lowest L/M ratio of any EHe studied so far. If a core-mass luminosity relation can legitimately be invoked for EHe stars (cf. Jeffery 1988, Saio 1988), it must be the lowest mass member of the group.

LSS 3184 has $T_{\rm eff}$ and $\log g$ very similar to two other stars with $n_{\rm H} \lesssim 0.01$, namely V652 Her as mentioned above (Lynas-Gray et al. 1984, Jeffery et al. 1986) and HD 144941 (Harrison & Jeffery 1997) (Table 2). It had previously been supposed that these two stars were intrinsically different from other EHe stars, *both* because they had comparatively high hydrogen abundances ($n_{\rm H} \sim 0.01$) *and* because of their lower L/M ratios. Moreover their CNO and other abundances are strikingly different from those of other EHes. It was consequently proposed that V652 Her (at least, cf. Jeffery 1984) had a different internal structure and evolutionary origin. However, with LSS 3184 having similar $T_{\rm eff}$ and $\log g$ to V652 Her and HD 144941, and the R CrB star DY Cen (Jeffery & Heber 1993) having a higher hydrogen abundance, such a hypothesis ceases to be defensible. The evolutionary process or processes (cf. Iben et al. 1996) which create EHes must be able to create stars with luminosities ranging from $3.0 \lesssim \log L/M \lesssim 4.5$, hydrogen abundances ranging from $< -4 \lesssim \log n_{\rm H} \lesssim -0.8$, and a considerable variation in the abundances of all major atomic species.

All three stars just discussed (LSS 3184, V652 Her and HD144941) are located in a high-gravity finger in $g - T_{\rm eff}$ space where radial pulsations driven by He^+ ionization occur because of high metal opacities around 10^6 K (Saio 1995, Fig. 4). Such pulsations are predicted to occur only if the metal abundance is sufficiently high. In the case of LSS 3184 our measurements of the metallicity give $Z \sim 0.007$, if we consider those species which contribute most to the opacity at 10^6 K. Thus LSS 3184 provides a crucial test of the opacity calculations;

Table 4. Other measured absorption lines in the spectrum of LSS 3184

Mu.	λ(Å)	W_λ	Note	Mu.	λ(Å)	W_λ	Note
He I							
12	4713.2	473		16	4120.9	578	
5	3964.7	462		50	4437.5	324	
52	4169.0	275		54	4024.0	46	
57	3935.9	236		61	3838.1	188	S III$_5$
He II							
1	4685.7	67					
C II							
1	4735.5	31		1	4738.0	18	
1	4744.8	51		1	4747.3	18	
4	3919.0	187	N II$_{17}$	4	3920.7	182	
6	4267.1	448	bl	12.02	4307.6	69	
13	3831.7	68		13	3835.7	59	
13	3836.7	15		27	4017.3	51	
28	4317.3	123	O II$_2$	28	4318.6	45	N III$_{10}$
28	4321.6	54	N III$_{10}$	28	4326.0	138	bl; O II$_2$
32?	3952.1	113		33	3876.1	82	bl
33	3876.5	222	bl	33	3879.6	72	
33	3880.6	73		33.01?	3868.9	51	
35.01	4077.7	72	bl	36	4075.9	319	bl; N II$_{38}$
36	4074.7	263	bl	37	3972.4	49	C II$_{38}$
37	3977.3	49	bl	37	3978.8	66	bl
37	3980.3	48		39	4411.3	194	bl
40	4409.2	34		40	4410.0	96	
41	4295.9	53		42	4291.8	51	C II$_{41}$
45	4368.3	29	C II$_{46}$	45	4369.9	14	
45	4372.4	154	bl; C II$_{46}$	45	4374.3	115	
45	4375.0	47	N II$_{16}$	45	4376.6	69	
49?	4625.6	37					
C III							
1	4650.3	128		5	4651.0	65	C III$_1$
5	4652.0	7		5	4663.6	24	
9?	4515.5	8	bl;cr	9?	4516.8	4	cr
14?	4382.9	26		16	4068.9	37	
18	4186.9	21		21?	4162.9	58	S II$_{44}$
N II							
6	3955.9	156		11	4654.5	50	
11	4667.2	67		11	4674.9	62	O II$_1$
14	4564.8	27		21	4459.9	34	
21	4477.7	78		21	4488.1	32	O II$_{104}$
21	4507.6	60		30	3838.4	64	S III$_5$
30	3855.1	121		30	3856.1	124	O II$_{12}$
38	4073.0	94	cr	38	4076.9	99	C II$_{36}$
38	4082.3	97		38	4095.9	102	O II$_{48}$
38	4087.3	67	O II$_{48}$	39	4039.3	44	
39	4044.8	99		43	4171.6	78	
43	4176.2	164		43.01	4131.8	124	
44	4110.0	76		44	4110.8	60	
48	4247.2	25	N II$_{21.02}$	49	4181.1	51	
49	4196.0	94	N III$_6$	49	4200.0	137	N III$_6$
49	4201.4	30		50	4156.7	133	bl; C III$_{21}$
50	4161.1	19		50	4173.6	211	
54.01	4508.8	32		55	4417.1	1.61	O II$_5$
57.01	4602.6	68	O II$_{93}$	57.01	4608.1	55	
58	4552.5	250	Si III$_2$	61	4694.6	118	
65	4124.1	80		65	4133.7	84	
65	4145.8	30	S II$_{44}$	68	4695.9	39	O II$_1$
68	4698.6	93	O II$_{25}$	68	4700.0	15	

Table 4. (continued)

Mu.	λ(Å)	W_λ	Note	Mu.	λ(Å)	W_λ	Note
N II							
68	4702.5	11		68	4704.2	12	
68	4706.4	3	cr	68	4709.6	38	N II$_{25}$
68	4718.4	16		68	4721.6	9	
72	3939.6	50		72	3940.7	44	
72	3941.2	40		74	4206.3	100	bl
74	4207.5	92		73	4154.8	39	
N III							
2	4634.1	19	cr	3?	4510.9	61	bl
3?	4518.2	16	cr	10?	4332.9	89	S III$_4$
O II							
1	4641.8	154	N III$_2$	1	4649.1	156	C III$_1$
1	4673.8	27	C III$_5$				
2	4336.9	54	N III$_{10}$	12	3864.6	13	bl
16	4347.4	90	bl?	19	4153.3	98	C III$_{21}$
20	4103.0	62	N III$_1$	21	4096.5	56	O II$_{48}$
41	4327.5	31	N III$_{10}$	41	4331.9	22	cr
48	4089.3	128	Si IV$_1$	49?	4083.9	21	O II$_{21}$
54	4294.8	29	S II$_{49}$	58	4701.2	14	Al III$_6$
77	4342.0	57	Si III$_{46}$	92	4610.1	20	
Ne II							
64?	4499.0	37					
Ca II							
1	3933.7	545		1	3968.5	322	
Al III							
9?	4364.6	30	Fe III$_4$				
Si III							
8.10?	4102.4	27		8.14	3924.5	57	
8.16?	4800.4	38		10.08?	3947.5	45	
15?	4554.0	30					
P III							
9?	3904.8	42					
S III							
7?	4439.9	12		8?	3986.0	58	
Fe III							
121?	4273.4	34		121?	4304.8	26	
121?	4310.4	30			4210.9	88	

Notes:

Mu	Multiplet
bl	two or more components of same multiplet
cr	cosmic ray

with $Z \sim 0.01$, models state that LSS 3184 should pulsate, with $Z \sim 0.004$ it should not. Certainly the amplitude of pulsations in LSS 3184 is much lower than in the more metal-rich V652 Her whilst the absence of pulsations in HD 144941 (Jeffery & Hill 1996b) has already been demonstrated to be due to its very low metallicity (Z = 0.0003, Harrison & Jeffery 1997). Therefore a precise measurement of the iron abundance from UV spectra and the construction of theoretical pulsation models using opacities tailored to the observed abundances would provide very powerful diagnostics both of stellar structure and atomic physics.

Table 5. Unidentified lines in the spectrum of LSS 3184. Wavelengths have been corrected for stellar motion to give laboratory wavelengths in air.

λ Å	W_λ mÅ	λ	W_λ	λ	W_λ
3897.0	183	3899.3	45	3915.4?	28
4015.9	41	4248.5	22	4259.6	55
4261.3	76	4292.3	137	4329.8	138

5. Conclusions

The analysis shows that LSS 3184 has a high carbon abundance typical of other EHes. It is extremely hydrogen deficient, hydrogen being present by less than one part in 10^4 by numbers. The evidence of the nitrogen and other metal abundances implies that the primordial metallicity of LSS 3184 was subsolar by ~ -0.5 dex, but that nitrogen and carbon have been enriched by CNO and 3α processing. The low primordial metallicity may be reflected in the lower amplitude of LSS 3184 pulsations relative to V652 Her, which are driven by iron-group opacities at $\sim 10^6$ K.

Acknowledgements. The authors are grateful to the referee, Bertrand Plez, for his remarks, and to UK PPARC's CCP7 for finance and software.

Appendix A: additional line measurements

A list of measured equivalent widths for identified lines which were not included in Table 1 is given in Table 4. Although exhaustive searches were made using published linelists, a significant number of lines, some relatively strong ($W_\lambda \sim 100$mÅ), eluded identification. A list of these, with laboratory wavelengths accurate to ± 0.1Å, is given in Table 5. At least two occur in the spectrum of LSE 78 (Jeffery 1993), and others also occur in spectra of the helium stars BD+10°2179 and V348 Sgr (Leuenhagen et al. 1994). Given that many lines which are normally not seen or are very weak in hydrogen-rich stars *are* observed in LSS 3184, it is likely that many belong to unclassified transitions of C II, N II, and O II.

References

Allard N., Artru M.-C., Lanz T., Le Dourneuf M., 1990, AAS 84, 563
Anders E., Grevesse N., 1989, Geochim. Cosmochim. Acta 53, 197
Barnard A.J., Cooper J., Shamey L.J., 1969, AA 1, 28
Barnard A.J., Cooper J., Smith E.W., 1974, JQSRT, 14, 1025
Barnard A.J., Cooper J., Smith E.W., 1975, JQSRT, 15, 429
Beauchamp A., Wesemael F., Bergeron P., Liebert J. Saffer R.A., 1996. Hydrogen-deficient stars, p. 295, eds. Jeffery C.S., Heber U., ASP Conf. Ser. Vol. 96
Becker S.R., Butler K., 1989, AA 209, 244
Becker S.R., Butler K., 1990, AA 235, 326
Bell K.L., Hibbert A., Stafford R.P., McLaughlin B.M., 1994. Physica Scripta 50, 343
Butler K. 1984, PhD Thesis, University College London
Drilling J.S., 1980, ApJ 242, L43
Drilling J.S., Hill P.W., 1986, Hydrogen-deficient stars and related objects, IAU Coll. 87, p. 499, Hunger K., Schönberner D. Rao N.K., Reidel, Dordrecht, Holland.
Hardorp J., Scholz M., 1970, ApJS 19, 193
Harrison P.M., Jeffery C.S., 1997, AA 323, 177
Heber U., Jonas G., Drilling J.S., 1986, Hydrogen-deficient stars and related objects, IAU Coll. 87, p. 67, Hunger K., Schönberner D. Rao N.K., Reidel, Dordrecht, Holland.
Holweger H., Heise C., Kock, M., 1990, AA 232, 510
Iben I. Jr., Tutukov A.V., Yungelson L.R., 1996. ApJ 456, 750
Jeffery C.S., 1984, MNRAS 210, 731
Jeffery C.S., 1988, MNRAS 235, 1287
Jeffery C.S., 1993, AA 279, 188
Jeffery C.S., 1996, Hydrogen-deficient stars, p. 152, eds. Jeffery C.S., Heber U., ASP Conf. Ser. Vol. 96
Jeffery C.S., Heber U., 1992, AA 260, 133
Jeffery C.S., Heber U., 1993, AA 270, 167
Jeffery C.S., Hill P.W., 1986, MNRAS 221, 975
Jeffery C.S., Hill N.C., 1996a, Hydrogen-deficient stars, p. 396, eds. Jeffery C.S., Heber U., ASP Conf. Ser. Vol. 96
Jeffery C.S., Hill P.W.: 1996b, The Observatory 116, 156
Jeffery C.S., Heber U., Hill P.W., 1986, Hydrogen-deficient stars and related objects, IAU Coll. 87, p. 101, Hunger K., Schönberner D., Rao N.K., Reidel, Dordrecht, Holland.
Kilkenny D., Koen C.: 1995, MNRAS 275, 326
Kodaira K., Scholz M.: 1970, AA 6, 93
Kurucz R.L.: 1979, ApJS 40, 1
Kurucz R.L., Peytremann E.: 1975, A Table of Semiempirical gf Values, SAO Special Report No. 362, Cambridge, Massachussets 02138
Leuenhagen U., Heber U., Jeffery C.S.: 1994, AAS 103, 445
Lynas-Gray A.E., Schönberner D., Hill P.W., Heber U.: 1984, MNRAS 209, 387
Möller R. U.: 1990, Diplom. Thesis, Universität Kiel
Peach G.: 1970, Mem. R. astr. Soc. 73, 1
Saio H.: 1988, MNRAS 235, 203
Saio H.: 1995, MNRAS 277, 1393
Stürenburg S., Holweger H., 1990, AA 237, 125
Wiese W.L., Smith M.W., Glennon B.M., 1966, Atomic Transition Probabilities, National Bureau of Standards, Washington
Wiese W.L., Smith M.W., Miles B.M., 1969, Atomic Transition Probabilities, National Bureau of Standards, Washington
Yan Y., Taylor K.T., Seaton M.J., 1987, J. Phys. B 20, 6399

This article was processed by the author using Springer-Verlag LaTeX A&A style file *L-AA* version 3.